NASA RADIATION PROTECTION RESEARCH FOR EXPLORATION MISSIONS

John W. Wilson[1], F. A. Cucinotta[2], Ram K. Tripathi[1], John H. Heinbockel[3], John Tweed[3], Christopher J. Mertens[1], Steve A. Walker[3], Steven R. Blattnig[1], Cary J. Zeitlin[4]

[1]*NASA Langley Research Center, Hampton VA 23681-2199 USA*
[2]*NASA Johnson Space Center, Houston, TX 77058 USA*
[3]*Old Dominion University, Norfolk VA 23529 USA*
[4] *Lawrence Berkeley National Laboratory, Berkeley, CA 94720 USA*

ABSTRACT

The HZETRN code was used in recent trade studies for renewed lunar exploration and currently used in engineering development of the next generation of space vehicles, habitats, and EVA equipment. A new version of the HZETRN code capable of simulating high charge and energy (HZE) ions, light-ions and neutrons with either laboratory or space boundary conditions with enhanced neutron and light-ion propagation is under development. Atomic and nuclear model requirements to support that development will be discussed. Such engineering design codes require establishing validation processes using laboratory ion beams and space flight measurements in realistic geometries. We discuss limitations of code validation due to the currently available data and recommend priorities for new data sets.

INTRODUCTION

Our early interest in transport code development paralleled the experimental studies of Walter Schimmerling et al. (1986) at the Lawrence Berkeley Laboratory and involved solving the Boltzmann transport equation for mono-energetic ion beams in the context of the continuous slowing down approximation (Wilson et al. 1984). The main computational limitation was found to be the inadequacy of available nuclear data through comparing computational results with the ionization data for a broad beam of ^{20}Ne ions (Wilson et al. 1984, Shavers et al. 1990, 1993). Emphasis was soon overtaken by the need to establish the scope of the GCR protection problem and marching procedures were used to get first order estimates of shielding requirements (Wilson et al. 1991). Testing the new computational marching model against atmospheric air shower data again pointed to the inadequacy of the available nuclear data (Wilson and Badavi 1986) and development of a semi-empirical nuclear model followed, leading to reduced computational errors (Wilson et al. 1987a, 1987b). The next dozen years emphasized spaceflight validation of the marching solution and nuclear model improvements (Badhwar et al. 1996, Shinn et al. 1998, Cucinotta et al. 1998, Wilson et al. 1995, 2006a, 2007, Hugger et al. 2003, Nealy et al. 2007). Advanced solution methods of the Boltzmann equation continued to develop (Wilson et al. 1994a,b) but only slowly after NASA interest in deterministic transport code and nuclear model development shifted in favor of Monte Carlo methods (Armstrong and Colburn 2001, Pinsky et al. 2001). Recent renewed interest within NASA for deterministic code development is giving new emphasis to improved solution methods (Wilson et al. 2004, 2005a, Tweed et al. 2005, 2006) with a renewed focus on nuclear modeling activity (Cucinotta et al. 1994, 1998, 2007, Norbury et al. 2007). As a result, recent developments mainly utilize the older semi-empirical NUCFRG2 model (Wilson et al. 1995, 2005b, Walker et al. 2005) with energy downshifts and momentum dispersion (Tripathi et al.

1994). Comparison of NUCFRG2 with other models and experiments are given by Zeitlin et al. (1997), Cucinotta et al. (2007), and Walker et al. (2005). As a result for the need to design and test new systems for future exploration in the low Earth orbit environment, there has been renewed interest in flight validation using International Space Station as a measurements platform (Hugger et al. 2003, Wilson et al. 2005b, 2007, Nealy et al. 2007). In the current report, we will review the current status of transport code development with emphasis on future needs.

DETERMINISTIC CODE DEVELOPMENT

The relevant transport equations are the linear Boltzmann equations derived on the basis of conservation principles (Wilson et al. 1991) for the flux density $\phi_j(\boldsymbol{x}, \boldsymbol{\Omega}, E)$ for particle type j as

$$\boldsymbol{\Omega}\bullet\boldsymbol{\nabla}\phi_j(\boldsymbol{x},\boldsymbol{\Omega},E)=\sum\int\sigma_{jk}(\boldsymbol{\Omega},\boldsymbol{\Omega}',E,E')\,\phi_k(\boldsymbol{x},\boldsymbol{\Omega}',E')\,d\boldsymbol{\Omega}'\,dE' - \sigma_j(E)\,\phi_j(\boldsymbol{x},\boldsymbol{\Omega},E) \quad (1)$$

where $\sigma_j(E)$ and $\sigma_{jk}(\boldsymbol{\Omega},\boldsymbol{\Omega}',E,E')$ are the shield media macroscopic cross sections. The $\sigma_{jk}(\boldsymbol{\Omega},\boldsymbol{\Omega}',E,E')$ represent all those processes by which type k particles moving in direction $\boldsymbol{\Omega}'$ with energy E' produce a type j particle in direction $\boldsymbol{\Omega}$ with energy E *(including decay processes)*. Note that there may be several reactions that produce a particular product, and the appropriate cross sections for equation (1) are the inclusive ones. Exclusive processes are functions of the particle fields and may be included once the particle fields are known. The total cross section $\sigma_j(E)$ with the medium for each particle type is

$$\sigma_j(E) = \sigma_{j,at}(E) + \sigma_{j,el}(E) + \sigma_{j,r}(E) \quad (2)$$

where the first term refers to collision with atomic electrons, the second term is for elastic scattering on the nucleus, and the third term describes nuclear reactions where we have ignored the minor nuclear inelastic processes (excitation). The corresponding differential cross sections are similarly ordered. Many atomic collisions (~10^6) occur in a centimeter of ordinary matter, whereas ~10^3 nuclear coulomb elastic collisions occur per centimeter, while nuclear reactions are separated by a fraction to many centimeters depending on energy and particle type. Solution methods first use perturbations based on the ordering of the cross sections with atomic interactions as the first physical perturbation with special methods used for neutrons for which atomic cross sections are zero.

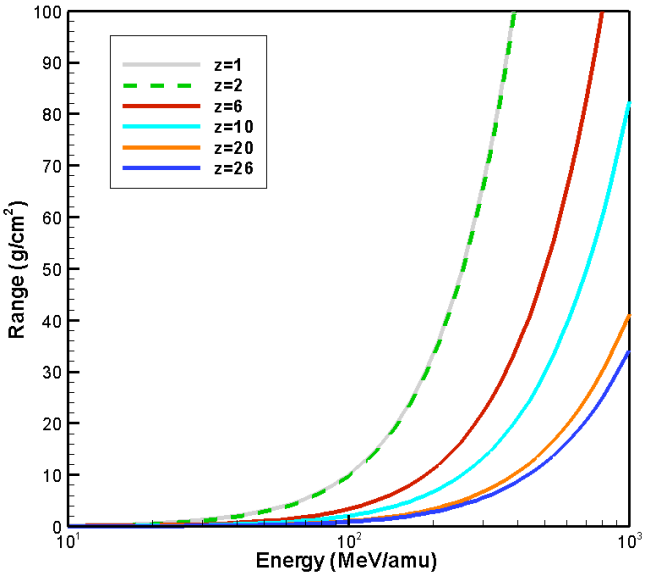

Fig. 1 Range of ions in aluminum.

We rewrite equation (1) in operator notation by defining a vector array field function as

$$\boldsymbol{\Phi} = [\phi_j(\boldsymbol{x}, \boldsymbol{\Omega}, E)] \quad (3)$$

the drift operator as

$$\boldsymbol{D} = [\boldsymbol{\Omega}\bullet\boldsymbol{\nabla}] \quad (4)$$

and the interaction operator as

$$\boldsymbol{I} = [\sum\int\sigma_{jk}(\boldsymbol{\Omega},\boldsymbol{\Omega}',E,E')\,d\boldsymbol{\Omega}'\,dE' - \sigma_j(E)] \quad (5)$$

with the understanding that $\boldsymbol{I}$ has three parts associated with atomic, elastic, and reactive processes as given in equation (2). Equation (1) is then rewritten as

$$[\boldsymbol{D}-\boldsymbol{I}_{at}-\boldsymbol{I}_{el}]\bullet\boldsymbol{\Phi} = \boldsymbol{I}_r\bullet\boldsymbol{\Phi} \quad (6)$$

where the first two physical perturbation terms are shown on the left-hand side and are represented by

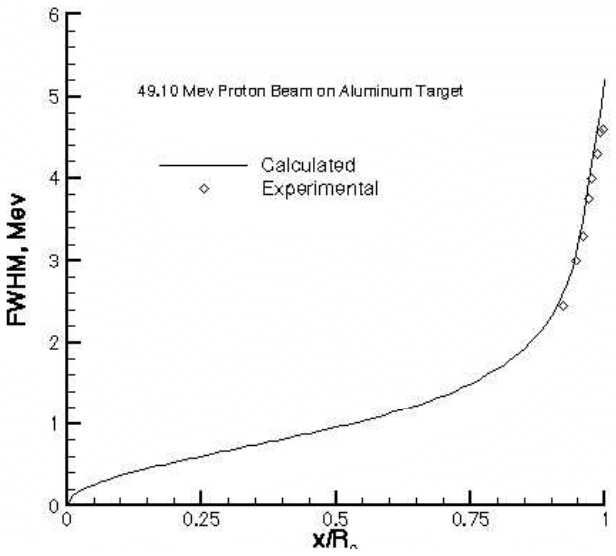

Fig. 2 FWHM of 49.1 MeV protons.

diagonal operators. The first order physical perturbation for atomic processes is solution of

$$[D - I_{at}] \bullet \Phi = 0 \tag{7}$$

using the moments methods, the solution can be approximated by

$$\Phi(z,E) = \exp[-(E - \langle E(z) \rangle)^2 / (2s^2(z))] / (\sqrt{(2\pi)}\, s(z)) \tag{8}$$

where the array of mean residual energies $\langle E(z) \rangle$ and the energy deviation $s(z)$ are evaluated using a second order Green's function (Wilson et al. 2002) and related to range and full width at half maximum (FWHM) shown in Figs. 1 and 2. Although straggling correction for the uncollided beam is important, it is negligible in the higher order terms compared to the energy dispersion in fragmentation.

The second order physical perturbation is the Coulomb scattering by the atomic nucleus as a solution of

$$[D - I_{el}] \bullet \Phi = 0 \tag{9}$$

and represented by Rutherford scattering modified by screening of the nuclear charge by the orbital electrons using the Thomas-Fermi distribution for the atomic orbitals. We will utilize the multiple Coulomb scattering solutions of Fermi given by

$$\Phi(z,r,\theta_r) = [\sqrt{3}\, w^2/2\pi z^2] \times \exp[-w^2(\theta_r^2/z - 3r\theta_r/z^2 + 3r^2/z^3)] \tag{10}$$

where z is the longitudinal distance, r is the lateral distance, θ_r is the angle to the longitudinal axis, and w^2 the array of appropriate diffusion coefficients. Strictly speaking, the solution applies only over intervals for which the variation in ion energy is small. It follows that the mean square angle (understood as a differential quantity) in traveling a distance dz is given from equation (10) as

$$\langle \theta_r^2 \rangle = 2\, dz/w^2 \tag{11}$$

Conversely, one finds for a uniform nuclear charge distribution shielded by a Thomas-Fermi atomic structure

$$\langle \theta_r^2 \rangle = dz\, (Z_P E_s/\beta pc)^2 / X_0 \tag{12}$$

so that

$$w^2 = 2X_0\, (\beta\, pc / Z_P E_s)^2 \tag{13}$$

where

$$E_s = \sqrt{(4\pi\, \mu_e^2/\alpha)} = 21.2 \text{ MeV} \tag{14}$$

with α the fine structure constant, p the ion momentum array, the array β of ion speeds relative to the speed of light c, Z_P the array of projectile charges, and X_0 is the electron radiation length in the material. The electron radiation length (g/cm^2) is given by

$$X_0^{-1} = 4\alpha\, (N_A/A)\, Z_T^2 r_0^2\, \ln(181 Z_T^{-1/3}) \tag{15}$$

with Avagadro's number N_A, A the molecular weight, and r_0 the classical electron radius. We will be using Schimmerling and coworkers modifications to Fermi's width formula (1986, Wong et al. 1989). Multiple Coulomb scattering played a critical role in prior experimental validation of the transport solutions (Shavers et al. 1990, 1993). An example of multiple Coulomb scattering is given in Fig. 3 showing the emerging ion angular distribution on the beam axis and off the beam axis for 600 A MeV iron ions in aluminum. The iron ions on the beam axis remain highly peaked in the forward direction while those that have scattered off axis exhibit wider angular divergence. In all cases the angular dispersion is small and clearly will be important only for the uncollided beam ions. Recent advances in coupling multiple Coulomb elastic scattering with first order transport processes (energy loss and straggling) is discussed in Mertens et al. (2007).

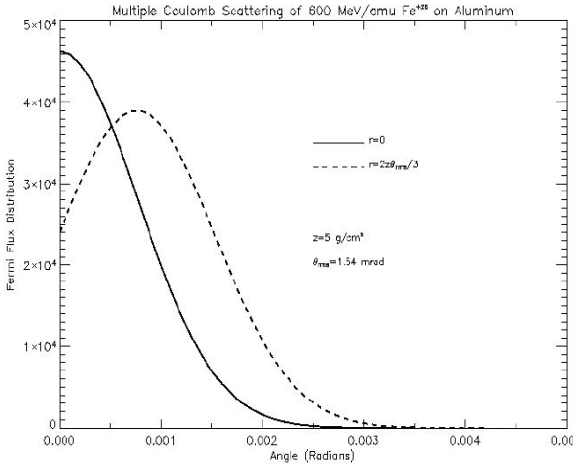

Fig. 3 Multiple Coulomb scattering of 600 A MeV iron ions in a 5 g/cm^2 aluminum target.

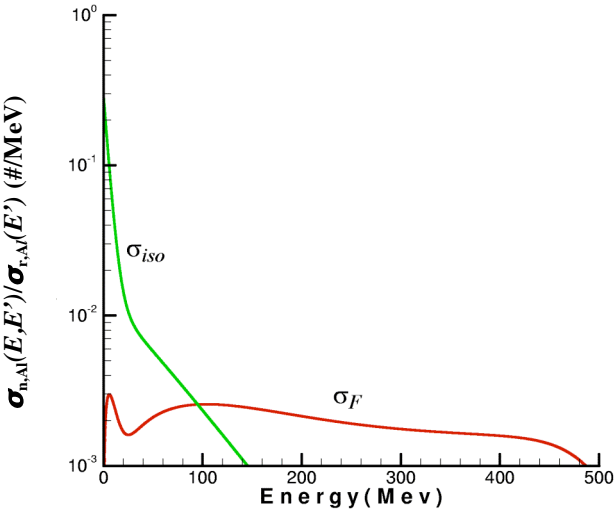

Fig. 4 Isotropic and forward neutron spectra produced by 500 MeV proton in aluminum.

The third order physical perturbation involves the nuclear reactive processes represented by the operator $\boldsymbol{I}_r$ of equation (6), rewritten as follows

$$[D - I_{at} - I_{el} + \sigma_r] \bullet \Phi = \{ \int \sigma_r(\Omega,\Omega',E,E') \, d\Omega' \, dE' \} \bullet \Phi \equiv \Xi_r \bullet \Phi \tag{16}$$

The off-diagonal nuclear reactive differential cross sections can be written in the following form

$$\sigma_{jk,r}(\Omega,\Omega',E,E') = \sigma_{jk,iso}(E,E')/4\pi + \sigma_{jk,for}(\Omega,\Omega',E,E') \tag{17}$$

where the first term is isotropic and associated with lower energy particles produced including target fragments and the second term is highly peaked in the forward direction and is associated mainly with direct quasi-elastic events and projectile fragmentation products (Wilson 1977, Wilson et al. 1988). Surprisingly, even nucleon-induced reactions follow this simple form and the isotropic term extends to relatively high energies (see Fig. 4). For nucleon induced reactions, the following form has been used in versions of FLUKA (Ranft 1980) as follows

$$\sigma_{jk,r}(\Omega,\Omega',E,E') = \nu_{jk}(E') \, \sigma_{jk,r}(E') f_{jk}(E,E') \times g_R(\Omega \bullet \Omega', E, A_T) \tag{18}$$

where $\nu_{jk}(E')$ is multiplicity and the Ranft factor used in FLUKA is

$$g_R(\Omega \bullet \Omega', E, A_T) = N_R \exp[-\theta^2/\lambda_R] \quad \pi/2 \geq \theta \geq 0 \tag{19}$$

and constant for larger values of production angle θ, N_R is normalization constant, and λ_R given by Ranft as

$$\lambda_R = (0.12 + 0.00036 A_T/E) \tag{20}$$

although new generalized fits are being derived. This separation in phase space will be further exploited in computational procedures.

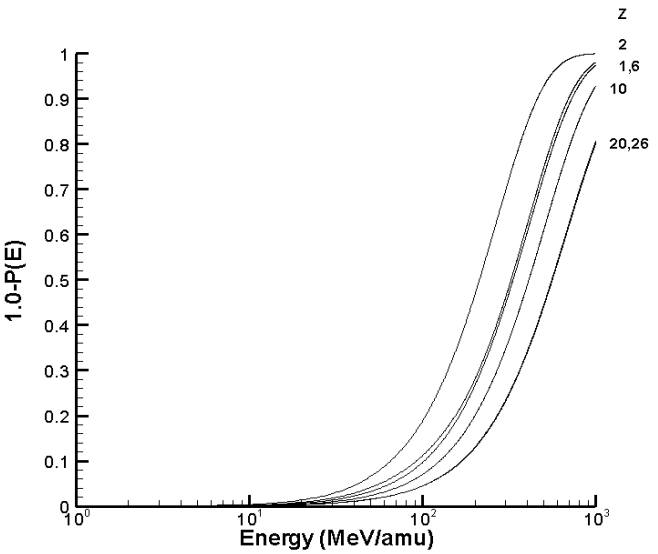

Fig. 5 Probability of nuclear reaction as a function of ion type and energy.

The heavy ion projectile fragment cross sections are further represented by

$$\sigma_{jk,for}(\Omega,\Omega',E,E') = \sigma_{jk,r}(E') \, N_t \exp[-2m\sqrt{(E'')}(1 - \Omega \bullet \Omega')/\varepsilon_{t,jk}] \times \exp[-(E + \lambda_{jk} - E')^2/2 \, \varepsilon_{jk}^2]/\sqrt{(2\pi\varepsilon_{jk}^2)} \tag{21}$$

where λ_{jk} is related to the momentum downshift, ε_{jk} is related to the longitudinal momentum width, $\varepsilon_{t,jk}$ is related to the transverse momentum width, and N_t is the transverse normalizing factor. Since the transverse width is small compared to the projectile and fragment energy the transverse function is highly peaked about the forward direction $(\Omega \bullet \Omega' \approx 1)$.

Atomic interactions limit the contributions of charged particles in the transport process. For example, the protons and alpha particles produced in aluminum below 100 A MeV contribute to the fluence only within a few centimeters of their collision source and the heavier ions are even more restricted (see Fig. 1). This is an important factor in that the transported secondary charged particle flux tends to be small at low energies and the role of additional nuclear reactions are likewise limited (see Fig. 5).

The reaction cross section is separated by equation (17) into isotropic and forward component for which equation (16) may be written as coupled equations

$$[D - I_{at} - I_{el} + \sigma_r] \bullet \Phi_{for} = \{ \int \sigma_{r,for}(\Omega,\Omega',E,E') \, d\Omega' \, dE' \} \bullet \Phi_{for} \equiv \Xi_{r,for} \bullet \Phi_{for} \tag{22}$$

and

$$[D - I_{at} - I_{el} + \sigma_r] \bullet \Phi_{iso} = \{ \int \sigma_r(\Omega,\Omega',E,E') \, d\Omega' \, dE' \} \bullet \Phi_{iso} + \{ \int \sigma_{r,iso}(\Omega,\Omega',E,E') \, d\Omega' \, dE' \} \bullet \Phi_{for} \equiv \Xi_r \bullet \Phi_{iso} + \Xi_{r,iso} \bullet \Phi_{for} \tag{23}$$

Equation (22) can be written as a Volterra equation (Wilson 1977, Wilson et al. 1991) and solved as

$$\Phi_{for} = [G + G \bullet \Xi_{r,for} \bullet G + G \bullet \Xi_{r,for} \bullet G \bullet \Xi_{r,for} \bullet G + \ldots] \bullet \Phi_B \tag{24}$$

for which the series can be evaluated directly as described elsewhere (Wilson et al. 1994a) and is amenable to numerical marching procedures.

The cross term in equation (23) gives rise to an isotropic source of light ions of only modest energies and neutrons. The high-energy portion of the isotropic spectra arises from multiple scattering effects and the Fermi motion of the struck nucleons within the nucleus. The low-energy isotropic spectra arise from decay processes of the struck nucleus. Spectral contributions to the Neumann series depend on the particle range and probability of surviving nuclear reactions that establish the functional form of the $\boldsymbol{G}$ matrix. The second term of the Neumann series is proportional to the probability of nuclear reaction that is limited by the particle range as discussed above and shown in Fig. 5. It is clear from Fig. 5 that those nuclear reactions for the charged particles below a few hundred A MeV are infrequent for which fast convergence of the Neumann series results. For the moment we will neglect the straggling and multiple-elastic processes to simplify the present explanation (these provide only minor corrections to space radiation exposures (Tweed et al. 2006) but are important in laboratory testing) and examine the remaining reactive terms of equation (22). The corresponding Volterra equation is given (Wilson 1977) by

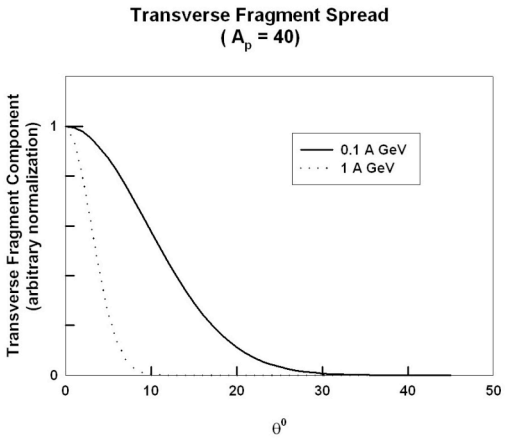

Fig. 6 Normalized transverse components for Ca fragmentation.

$$\phi_j(\boldsymbol{x},\boldsymbol{\Omega},E) = \{S_j(E_\gamma)P_j(E_\gamma)\,\phi_j(\boldsymbol{\Gamma}(\boldsymbol{\Omega},\boldsymbol{x}),\boldsymbol{\Omega},E_\gamma) + \Sigma\int_E^{E_\gamma} dE' A_j P_j(E') \int_{E'}^{\infty}\int_{4\pi} dE''d\boldsymbol{\Omega}'\,\sigma_{jk,for}(\boldsymbol{\Omega},\boldsymbol{\Omega}',E',E'') \times \phi_k(\boldsymbol{x}+[R_j(E) - R_j(E')]\boldsymbol{\Omega},\boldsymbol{\Omega}',E'')\}/\,S_j(E)P_j(E) \tag{25}$$

where $\phi_j(\boldsymbol{x},\boldsymbol{\Omega},E)$ in equation (25) represents the j^{th} component of the forward flux, $\boldsymbol{\Gamma}$ is the point on the boundary connected to $\boldsymbol{x}$ along $-\boldsymbol{\Omega}$ ($\boldsymbol{\Gamma}_{\boldsymbol{\Omega},\boldsymbol{x}}$ in Fig. 7), $E_\gamma = R_j^{-1}[\rho - d + R_j]$, ρ is the projection of $\mathbf{x}$ onto $\boldsymbol{\Omega}$, and d is the projection of $\boldsymbol{\Gamma}$ onto $\boldsymbol{\Omega}$. Equation (24) results from the Neumann series solution to equation (25). In the past we have expanded the angular integral over $\boldsymbol{\Omega}'$ asymptotically(Wilson and Khandelwal 1974) and implemented a solution as a marching procedure (HZETRN, Wilson and Badavi 1986), as a perturbation expansion (Wilson et al. 1984), and by non-perturbative approximation (Wilson et al. 1994a) resulting in three distinct methods to evaluate the first order asymptotic terms, all of which have had extensive experimental validation (Shavers et al. 1993, Wilson et al. 1998, Shinn et al. 1998). A typical lowest order asymptotic solution of equation (25) is shown in Figs. 8 and 9 for a high energy Fe^{56} ion incident on PMMA. Independent of the method used to evaluate the lowest order term, the first correction term is found by replacing the fluence in the integrand of equation (25) by the lowest order asymptotic solution $\phi_{k,o}(\boldsymbol{x},\boldsymbol{\Omega}',E'')$ as

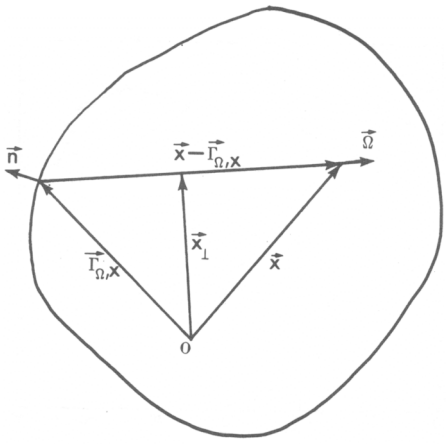

Fig. 7 Geometric relations of quantities useful in solving equation (25).

$$\phi_j(\boldsymbol{x},\boldsymbol{\Omega},E) = \{S_j(E_\gamma)P_j(E_\gamma)\,\phi_j(\boldsymbol{\Gamma}(\boldsymbol{\Omega},\boldsymbol{x}),\boldsymbol{\Omega},E) + \Sigma\int_E^{E_\gamma} dE' A_j P_j(E') \int_{E'}^{\infty}\int_{4\pi} dE''d\boldsymbol{\Omega}'\,\sigma_{jk,for}(\boldsymbol{\Omega},\boldsymbol{\Omega}',E',E'') \times \phi_{k,o}(\boldsymbol{x}+[R_j(E) - R_j(E')]\boldsymbol{\Omega}',\boldsymbol{\Omega}',E'')\}/\,S_j(E)P_j(E) \tag{26}$$

where $\phi_j(\boldsymbol{x},\boldsymbol{\Omega},E)$ is found as an integral over the neighborhood of rays centered on $\boldsymbol{\Omega}$ using the lowest order asymptotic solution $\phi_{k,o}(\boldsymbol{x},\boldsymbol{\Omega}',E'')$ along an adjacent ray directed along $\boldsymbol{\Omega}'$. Note that the boundary condition reached along $-\boldsymbol{\Omega}'$ enters through the lowest order asymptotic approximation and the angular integral correction in equation (25) is determined by the homogeneity and angular dependence of the space radiation and radius of curvature of the bounding material as we have shown long ago (Wilson and Khandelwal 1974, Wilson 1977). These are the determinant factors of the magnitude of the first order asymptotic correction that is anticipated to be very small for human rated systems (large radius of curvature) in space radiation that is homogeneous and isotropic in most applications (Wilson et al. 1991, Wilson et al. 1994b).

In a region of small radius of curvature the specific flux components near the site of evaluation will be missing contributions along adjacent rays that do not compensate losses along the ray on which the solution is evaluated representing the losses due to leakage. (Note, an asymptotic treatment of such small angle dependent

phenomena is the only useful approach circumventing large discretization errors.) This computational procedure is only a small addition to prior code development and will have little impact on computational efficiency. The angular dependence of the integral kernel of equation (26) is controlled by the forward reactive cross section $\sigma_{jk,for}(\Omega,\Omega',E',E'')$ with its highly peaked structure given by equations (18) or (21) depending on particle type. The angular dependence of the forward peak of fragmenting Ca ions at 100 and 1,000 A MeV is shown in Fig. 6. The low-energy ions with limited range have transverse components on the order of 10 degrees reducing to a few degrees at high energies. It should be clear that the added divergence added by multiple Coulomb scattering of such fragments (Fig. 3) is negligible to the large angular widths of the fragmentation event (Fig. 6) further justifying equation (25) in space applications.

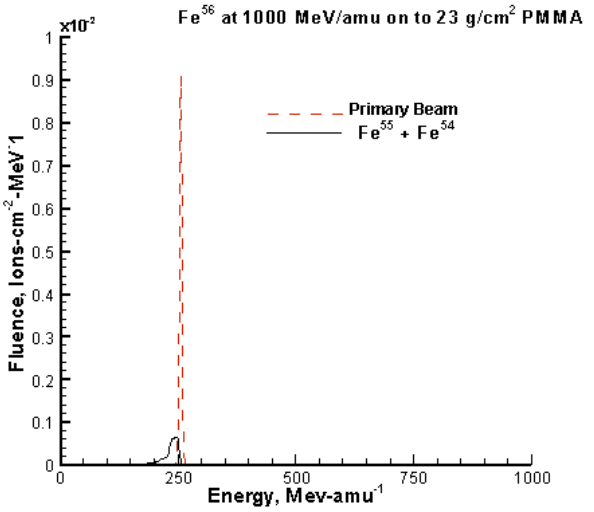

Fig. 8 Iron ion spectra after 23 g/cm^2 of PMMA.

Note that the low energy ions have limited range and will contribute little to the transported flux (see Fig. 1) or nuclear reactions (see Fig. 5). The higher energy ions, with their much longer pathlengths giving more important contributions, are related to only a very small angle of acceptance (few degrees) at the boundary. The form of the kernel leads directly to a Gauss-Hermite expansion and evaluation over the angle of production. Although the neutron Neumann series for the forward components converge more slowly since their contribution to the neutron flux is not limited by atomic interactions these higher energy neutrons will be adequately evaluated by similar procedures. Higher order asymptotic terms can be evaluated with similar iteration of equation (26) if required but all indications are that the first such correction will be small for most space radiation applications. This leaves the diffuse components of neutrons and light ions produced from the collision of the forward components and transported by equation (23) to be resolved (see for example, Clowdsley et al. 2000, 2001).

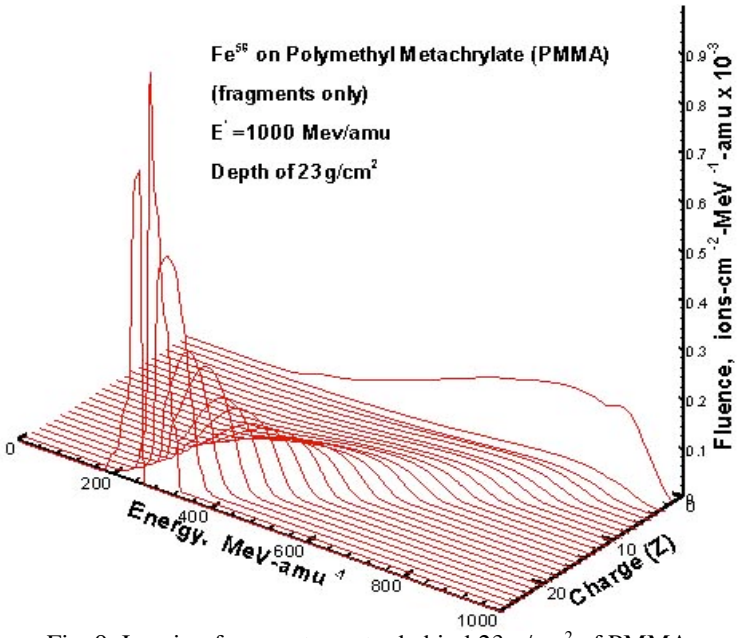

Fig. 9 Iron ion fragment spectra behind 23 g/cm^2 of PMMA.

The transport of the low-energy neutron and light-ion isotropic sources in equation (23) dominates the solution below about 70 A MeV (see Fig. 4). In this region light-ion transport is completely dominated by the atomic interaction terms and only a very small fraction have nuclear reactions making only minor contributions to the particle fields. This is especially true for the target fragments that can be solved in closed form including transition effects near boundaries of dissimilar materials (Wilson 1977, Cucinotta et al. 1991). The transport solution for the isotropic ion source terms to the lowest order perturbation is given by

$$\phi_{j,isoo}(\mathbf{x},\Omega,E) = \Sigma \int_E^{E_\gamma} dE' A_j P_j(E') \int_{E'}^{\infty} \int_{4\pi} dE'' d\Omega' \, \sigma_{jk,iso,r}(\Omega,\Omega',E',E'') \, \phi_{k,for}(\mathbf{x}+[R_j(E) - R_j(E')]\Omega,\Omega',E'')/ S_j(E)P_j(E) \qquad (27)$$

and will give highly accurate solutions to equation (23) since very few of the ions will have reactions (see Fig. 5), but could be easily corrected using the HZETRN light-ion propagator applied to the diffusive source terms. Note the E' integral effectively sums the ion source terms along direction Ω from the boundary to $\mathbf{x}$. Also, the nuclear survival terms $P_j(E)$ are all near unity (see Fig. 5 showing $1 - P_j(E)$).

The neutron transport is unhindered by atomic interaction (that is, neutron interaction with the atomic electrons). As a result neutron flux values are dominated by elastic and reactive nuclear processes. We further expand equation (23) for the single neutron component as

$$[\boldsymbol{\Omega}\bullet\boldsymbol{\nabla} + \sigma_n]\,\phi_n(\boldsymbol{x},\boldsymbol{\Omega},E) = \int\sigma_{nn}(\boldsymbol{\Omega},\boldsymbol{\Omega}',E,E')\,\phi_n(\boldsymbol{x},\boldsymbol{\Omega}',E')\,d\boldsymbol{\Omega}'\,dE' + [\boldsymbol{\Xi}_{r,iso}\bullet\boldsymbol{\Phi}_{for} + \boldsymbol{\Xi}_r\bullet\boldsymbol{\Phi}_{(27)}]_n \qquad (28)$$

where the last term is from coupling to the solution of equation (27) and is expected to make only small contributions to the neutron flux. In earlier work, we have approached solution of equation (28) using multigroup methods assuming a two-stream (forward/backward) approximation (Clowdsley et al. 2000) with limited success. A comparison of various methods (fb, Pn, Sn, and Monte Carlo) of direct solution of equation (28) is given by Heinbockel et al (2003) and shown in Fig. 10. The Sn method treated only the neutrons below 20 MeV. One problem with the fb and Pn methods is the approximations tend to fail at the higher energies since the elastic cross sections in HZETRN are poorly represented at higher energies. Since the solution above 25 MeV is dominated by nonelastic processes, a perturbation approach is taken to circumvent limitations in the high energy elastic cross section representations (Wilson et al. 1991).

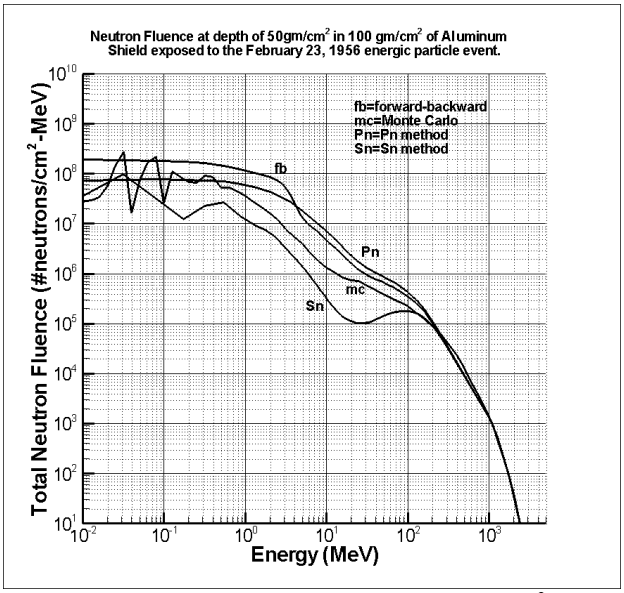

Fig. 10. Total neutron fluence at depth of 50 g/cm^2 in 100 g/cm^2 of aluminum shield exposed to the February 23, 1956 solar particle event.

The first term for diffusive neutron transport uses the lowest order perturbation similar to equation (27) given as

$$\phi_{n,iso}{}^{o}(\boldsymbol{x},\boldsymbol{\Omega},E) = \Sigma\int_0^{\rho-d} dx'\,exp[-\sigma_n(E)\,x']\int_{E'}^{\infty}\int_{4\pi} dE''d\boldsymbol{\Omega}'\;\boldsymbol{\sigma}_{jkisor}(\boldsymbol{\Omega},\boldsymbol{\Omega}',E',E'')\;\phi_{k,for}(\boldsymbol{x}-x'\boldsymbol{\Omega},\boldsymbol{\Omega}',E'') \qquad (29)$$

where $\rho-d$ is the distance along $-\boldsymbol{\Omega}$ from $\boldsymbol{x}$ to the boundary, x' is the distance from $\boldsymbol{x}$ to the source point along $-\boldsymbol{\Omega}$, and $\sigma_n(E)$ is the total neutron cross section. Note that equations (27) and (29) transport all particles associated with the collisions of the forward component $\boldsymbol{\Phi}_{for}$ found as solution to equation (24). The second collision term associated with the diffuse charged particle field given by equation (27) is negligible but additional source terms from the lowest-order diffuse neutron solution given by equation (29) provides an additional strong source of diffuse neutrons. The added transport of these neutrons is given by

$$[\boldsymbol{\Omega}\bullet\boldsymbol{\nabla} + \sigma_n(E)]\phi_{n,iso}{}^{1}(\boldsymbol{x},\boldsymbol{\Omega},E) = \int\boldsymbol{\sigma}_n(\boldsymbol{\Omega},\boldsymbol{\Omega}',E,E')d\boldsymbol{\Omega}'dE'\phi_{n,iso}{}^{1}(\boldsymbol{x},\boldsymbol{\Omega}',E') + \int\boldsymbol{\sigma}_{n,r}(\boldsymbol{\Omega},\boldsymbol{\Omega}',E,E')d\boldsymbol{\Omega}'dE'\phi_{n,iso}{}^{o}(\boldsymbol{x},\boldsymbol{\Omega}',E') \qquad (30)$$

where $\phi_{n,iso}{}^{1}(\boldsymbol{x},\boldsymbol{\Omega},E)$ is the remaining diffuse neutron component. The source term to the far right of equation (30) have been solved in exact 3D geometry and the energy spectrum is much degraded for the source term in equation (29). Typical spectra of the sources in equations (29) and (30) are compared in Fig. 11. The spectral properties of the second collision source terms of equation (30) result from terms like

$$f_1(E) = \int f(E,E')\,f_{iso}(E',\,500\text{ MeV})\,dE' \qquad (31)$$

It is clear that the diffuse spectra of neutrons from this term are highly degraded in energy for which Sn, Pn, or fb approximations are fully applicable and our final attention turns to solution of equation (30). Note that the software prepared for equation (30) is also applicable to nuclear reactor shielding issues with appropriate source terms. This is the typical nuclear engineering problem for which a multitude of methods have been developed such as the Sn, multigroup, and collocation methods already applied to HZETRN. It is mainly a question of computational efficiency and we continue to investigate this issue.

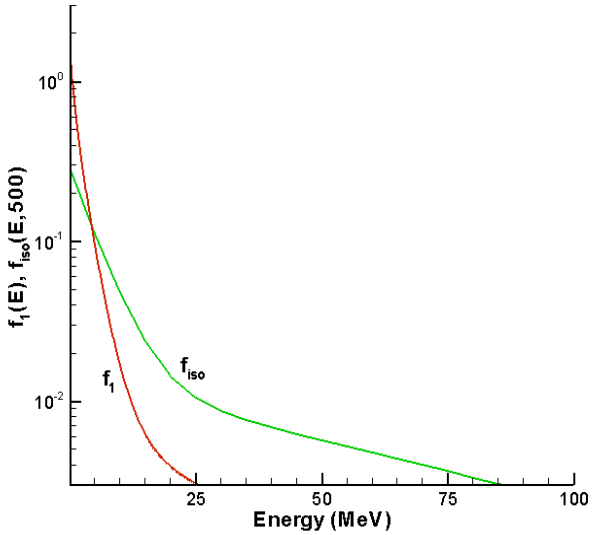

Figure. 11. Second collision neutron spectrum f1(E).

Although, equation (30) exhibits behavior similar to thermal diffusion there are strong differences between thermal and neutron diffusive processes. Thermal diffusion at ordinary temperatures has minor leakage through near boundaries since radiative processes are proportional to T^4 (in the absence of convection) leaving lateral diffusion an important process at low temperatures. In distinction, neutron diffusion is dominated by leakage at near forward and backward boundaries in penetrating spacecraft walls and lateral diffusion plays a minor role. Generally, low-energy neutron leakage is a dominant process within 15-20 g/cm^2 of the bounding surface in most materials. Since human rated systems have shielding of large radius of curvature and small thickness (4-20 g/cm^2) to radius ratio as determined by living and working space requirements, it approximates a connected system of flat plates for which leakage at forward and backward boundaries dominates the transport. In this limit the transport simplifies to a connected set of 1D transport problems with leakage at the back and forward boundaries (Clowdsley et al. 2000, 2001).

It is well established that the light ions produced in spacecraft materials are well described by current nuclear models so long as cluster processes are included as shown in Figs. 12 and 13. Curve B in the figures include the direct processes leading to light ions including direct knockout and de-excitation processes while curve A includes cluster processes with comparisons to Badhwar's PHIDE detector on Shuttle flight STS-48. Such solutions for charged particles are enhanced by the transport being dominated by atomic interactions. Neutron transport includes no atomic processes and greater demands on knowledge of nuclear processes and transport descriptions are traditionally problematic (see Fig. 10). The approach taken here of performing a first order Neumann perturbation as in equation (29) followed by a diffusion description in equation (30) is a reasonable next step and shows reasonable success in comparison with experimental flight data, see Fig. 14 (Getselev et al. 2004). Shown in the figure are measurements using photo-emulsion using two techniques (Li-6 loading and proton recoil methods) and a fission foil stack interleaved with nuclear track detectors. Also shown in the figure are Monte Carlo calculations accounting only for the GCR proton spectra that is expected to underestimate the spectrum especially at energies below 100 MeV. The geometry of the ISS was simplified in the Monte Carlo result and the only guidance we had was that the shielding was aluminum of 20-40 g/cm^2 thickness. In our simulations we included the full GCR spectrum, trapped protons and albedo neutrons for aluminum

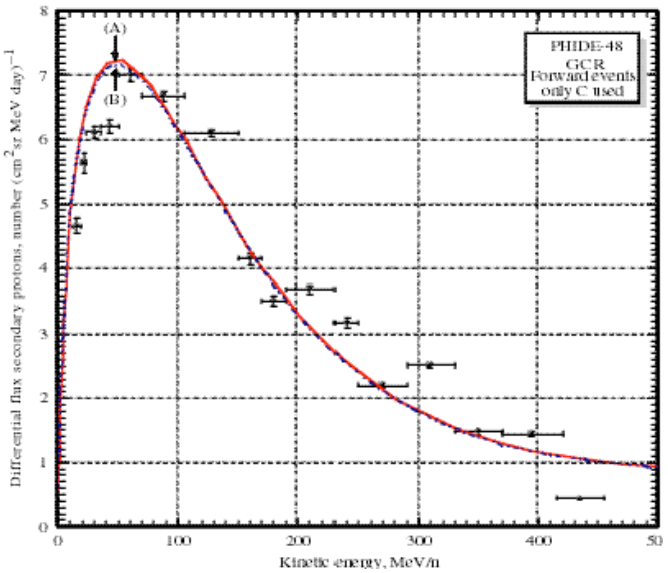

Fig. 12. Observed and calculated proton spectra.

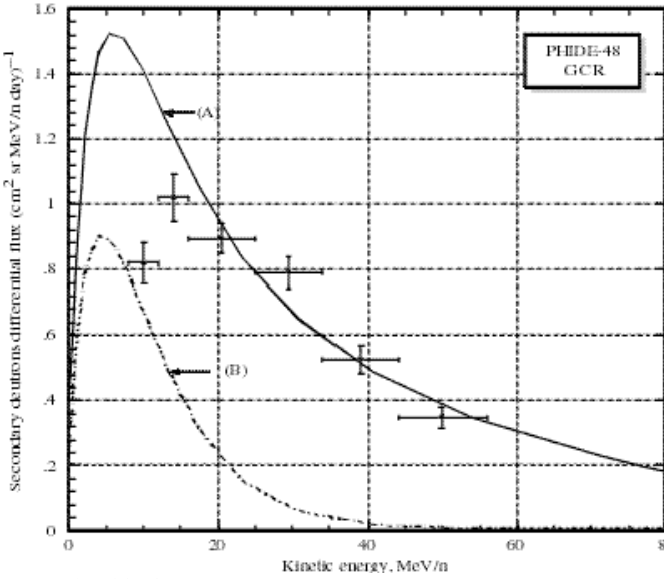

Fig. 13. Observed and calculated deuteron spectra.

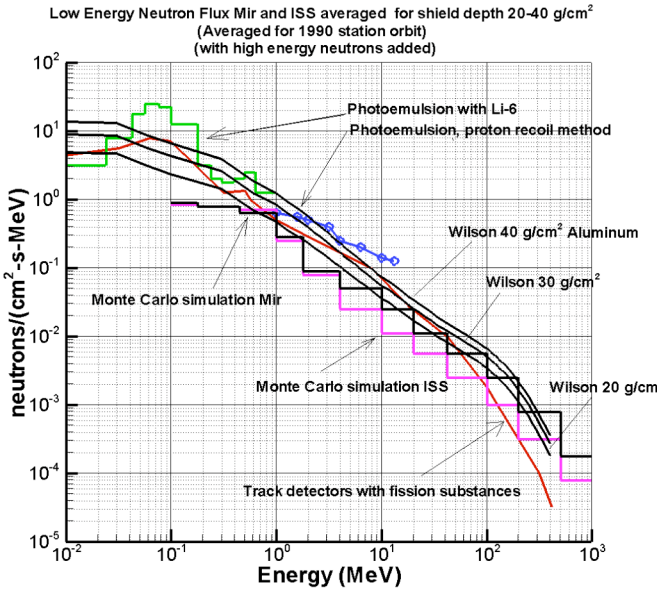

Fig 14. Observed and calculated neutron spectra.

spheres of thickness 20, 30, and 40 g/cm^2 in the comparisons. Clearly, the comparisons in the figure are very encouraging but an improved geometry definition is required to assess the accuracy of current transport methods.

FUTURE DEVELOPMENTS

In the past there has been a bifurcation in code development with codes used in space radiation studies relying on marching procedures and laboratory validation depending on Green's function solutions. The HZE Green's function has been well defined and tested in laboratory validation and directly relatable to the HZE portion of the space radiation shielding problem but the coupling to the light-ion/neutron propagation needs further investigation as does the light-ion/neutron Green's function.

Recent studies of the HZE Green's function have shown that straggling, energy downshifts, and energy dispersion are negligible in space radiation transport but have important consequences in laboratory experiments (Tweed et al. 2006b, Walker et al. 2006). Similarly for multiple scattering effects as discussed above and elsewhere (Tweed et al. 2006, Mertens et al. 2007). This allows the first order HZE Green's function derived many years ago ignoring these second order effects (Wilson et al. 1991, Chun et al. 1996) to be used in developing a new space radiation shielding code. The first work element is to develop an adequate Green's function based light-ion/neutron propagator based on the 2005 HZETRN formalism (Wilson et al. 2006) that is applicable to solution of equation (26) as well through substitution of only forward components in lowest order asymptotic approximation.

We specialize to solution along a ray Ω directed along the x-axis for which the Boltzmann equation within the continuous slowing down approximation assuming particles are produced in the forward direction (that is, lowest order asymptotic approximation)

$$[\partial_x - A_j^{-1}\partial_E S_j(E) + \sigma_j]\,\phi_j(x,E) = \Sigma_k \int \sigma_{jk}(E,E')\,\phi_k(x,E')\,dE' \tag{32}$$

where $\sigma_{jk}(E,E')$ are approximated for nucleons by the multiplicities of Ranft (1980), Bertini et al. (1972), and quasi-elastic contribution as described by Wilson et al. (1991). An immediate problem is the near singular nature of the differential operator and transformation from energy to residual range coordinates as we did in developing the Green's function greatly relieves this problem (Wilson et al. 1991). Unlike the Green's function development, numerical procedures are simplified by introducing only a single residual range coordinate for all ions and the residual proton range r is used as this common coordinate as

$$r = \int_0^E dE'/S(E') \tag{33}$$

and residual range of other particle types is related as $\nu_j\, r_j \approx r$ which fails at low energies corresponding to low residual range due to electron capture into atomic orbitals characteristic to each ion type. The corresponding transport equation is

$$[\partial_x - \nu_j\,\partial_r + \sigma_j(r)]\,\psi_j(x,r) = \Sigma_k \int_r^\infty (\nu_j/\nu_k)\,s_{jk}(r,r')\,\psi_k(x,r')\,dr' \tag{34}$$

where scaled flux is now (ν_j for neutral particles such as neutrons are taken as unity in scaling relations, Wilson et al. 1991)

$$\psi_j(x,r) = \nu_j\, S(E)\,\phi_j(x,E) \tag{35}$$

and the scaled differential cross sections are

$$s_{jk}(r,r') = S(E)\,\sigma_{jk}(E,E') \tag{36}$$

We will use the Voltera equation as derived by Wilson et al. (1991) arrived at by inverting the differential operator (Wilson et al. 1977, 1989,1991) of equation (34) as

$$\psi_j(x,r) = \exp[-\zeta_j(r,x)]\,\psi_j(0,r+\nu_j x) + \Sigma_k \int_0^x \int_{r+\nu_j x'}^\infty \exp[-\zeta_j(r,x')](\nu_j/\nu_k)\,s_{jk}(r+\nu_j x',r')\,\psi_k(x-x',r')\,dr'\,dx' \tag{37}$$

where the exponential is the integrating factor related to attenuation of the j type ions with

$$\zeta_j(r,x) = \int_o^x \sigma_j(r+\nu_j x')\,dx' \tag{38}$$

and is the particle extension coefficient. The Volterra equation (37) can be solved either as a Neumann series or by numerical marching procedures. Note that the inverse mapping is taken as

$$\phi_j(x,E) = A_j\,\psi_j(x,r)/S_j(E) \tag{39}$$

to guarantee the equilibrium solution given as equation (36) at low energies away from the boundaries (note, the proton stopping power is used in case of unscaling the neutron flux).

The Green's function associated with equation (34) relates the solution $\psi_j(x,r)$ to the boundary condition $\psi_j(0,r)$ as given by

$$\psi_j(x,r) = \Sigma_k \int G_{j,k}(x,r,r') \, \psi_j(0,r') \, dr' \tag{42}$$

resulting in the following equation for the Green's function

$$[\partial_x - \nu_j \, \partial_r + \sigma_j(r)] \, G_{j,k}(x,r,r') = \Sigma_k \int_r^{\infty} (\nu_j / \nu_k) s_{jk}(r,r'') \, G_{k,m}(x,r',r'') \, dr'' \tag{43}$$

where $G_{j,k}(x,r,r')$ approaches a delta function in r - r′ and j,k at the boundary. Functionally $G_{j,k}(x,r,r')$ satisfies a Boltzmann equation as does $\psi_j(x,r)$ and can be solved by similar procedures.

FUTURE NEEDS

From a transport perspective, the individual physical processes are well developed but there remain some tasks to smoothly integrate these methods into well-defined and efficient computational procedures. Primary uncertainties remain in the nuclear cross sections required to support the transport capability. An adequate neutron scattering database for which the above solution techniques were designed to minimize the impact of poor cross section definition above 25 MeV. Even below 25 MeV, the cross sections currently integrated into the transport procedures are of limited accuracy (Wilson et al. 1991) and major improvements can be made in both total and differential cross sections. The fragmentation cross sections are mainly based on the NUCFRG2 and an upgrade to more accurate quantum mechanical models is necessary. Continued testing against laboratory and spaceflight measurements is a necessary requirement for progress.

CONCLUSIONS

The current approach to solving the Boltzmann equation has been developing over 30 years following on the defining papers of Wilson and Khandelwal (1974) and Wilson (1977) with a major milestone in the development in the comprehensive report by Wilson et al. (1991). At this point in the development, an array of methodologies have been defined to treat the coupled solutions in a consistent way as to allow approach to a final development meeting all of the requirements of NASA in both space exposures to protect the astronauts and equipment on future missions as well as defining laboratory ion beam qualities supporting NASA radiobiological studies.

REFERENCES

Armstrong, T.W., Colburn, B.L. Predictions of secondary neutrons and their importance to radiation effects inside the international space station. *Radiat. Meas.* **33**: 229-234; 2001.

Badhwar, G.D., Patel, J.U., Cuccinotta, F.A., Wilson, J.W., Measurements of the secondary particle energy spectra in the Space Shuttle, *Rad. Meas*., **24**: 129–138; 1995

Badhwar, G.D., et al., In-flight radiation measurements on STS-60. *Radiat. Meas*. **26**:17-34; 1996.

Badhwar, G.D., et al. *Radiat. Meas*. **33**:235-241; 2001.

Bertini, H.W.. Guthrie, M.P., Culkowski, A.H. *Nonelastic Interactions of Nucleons and π-Mesons with Complex Nuclei at Energies Below 3 GeV*. ORNL TM-3148, 1972.

Chun, S.Y., Khandelwal, G.S., Wilson, J.W., A Green's function method for high charge and energy ion transport. *Nucl. Sci. & Eng*. 122: 267-275; 1996.

Clowdsley, M.S., et al. A comparison of the multigroup and collocation methods for solving the low-energy neutron Boltzmann equation. *Can. J. Phys*. **78**: 45-56; 2000.

Clowdsley, M.S., Wilson, J.W., Shinn, J.L., Badavi, F.F., Heinbockel, J.H., Atwell, W., *Neutron environment calculations for low Earth orbit*. SAE 01ICES2327, 2001.

Cucinotta, F. A.; Katz, R.; Wilson, J. W.; Townsend, L. W.; Shinn, J. L.; and Hajnal, F., Biological effectiveness of high-energy protons: Target fragmentation. *Radiation Research* **127**:130-137; 1991.

Cucinotta, F. A., and R. R. Dubey, Alpha-Cluster Description of Excitation Energies in ^{12}C (^{12}C, 3α) X at 2.1A GeV, *Phys. Rev*., **C50**: 979–984; 1994.

Cucinotta, F. A.; Wilson, J. W.; Shinn, J. L.; and Tripathi, R. K: Assessment and Requirements of Nuclear Reaction Data Bases for GCR Transport in the Atmosphere and Structures, *Adv. Space Res*., **21**(12): 1753-1762 1998;

Cucinotta, F.A., Wilson, J.W., Saganti, P., Hu, X. Kim, M.Y., Cleghorn, T., Zeitlin, C.E., Tripathi, R.K., Isotopic dependence of GCR fluence behind shielding. *Radiat. Meas.* In press, 2007.

Getselev, I., Rumin, S., Sobolevsky, N., Ufimtsev, M., Podzolko, M., Absorbed dose of secondary neutrons from galactic cosmid rays inside the international space station. *Adv. Space Res*. **34**: 1429-32; 2004.

Heinbockel, J.H., Feldman, G.A., Wilson, J.W., Singleterry, R.C., Clowdsley, M.S., Solutions to the low energy neutron Boltzmann equation for space applications. SAE 03ICES339, 2003.

Hugger, C.P., Nealy, J.E., Clowdsley, M.S., Wilson, J.W., Qualls, G.D., Atwell, W., Cucinotta, F.A., Golightly, M.J., Semones, E., Shavers, M.R., *Preliminary Evaluation of an ISS Radiation Shielding Model*. AIAA 2003-6620, 2003.

Mertens, C.J., Wilson, J.W., Walker, S.A., Tweed, J., Coupling of multiple Coulomb scattering and energy loss and straggling in HZETRN. *Adv. Space Res*. In press, 2007.

Nealy, J.E., Cucinotta, F.A., Wilson, J.W., Badavi, F.F., Dachev, Ts.P., Tomov, B.T., Walker, S.A., De Angelis, G., Blattnig, S.R., Atwell, W., Pre-engineering spaceflight validation of environmental models and the 2005 HZETRN simulation code. Adv. Space Res. In press, 2007.

Norbury, J.W., Dick, F., Tripathi, R.K., Eta-meson production in proton-proton collisions. NASA TP-in press, 2007.

Pinsky, L., Carminati, F., Ferrari, A. Simulation of space Shuttle neutron measurements with FLUKA. *Radiat. Meas***. 33**: 335-339; 2001.

Ranft, J. The FLUKA and KASPRO Hadronic Cascade Codes. *Computer Techniques in Radiation Transport and Dosimetry,* W. R. Nelson and T.M. Jenkins, eds, Plenum Press, pp. 339-371, 1980.

Schimmerling, W., Rapkin, M., Wong, M., Howard, J. The propogation of relativistic heavy ions in multielement beam lines. *Medical Phys*. **13**: 217-228; 1986.

Shavers, M. R., Curtis, S.B., Miller, J., Schimmerling, W. The fragmentation of 670A MeV Neon-20 as a function of depth in water. II. One-generation transport theory. *Radiat. Res*. **124**: 117-130; 1990.

Shavers, M. R., Frankel, K., Miller, J., Schimmerling, W., Townsend, L. W., Wilson, J. W., The Fragmentation of 670 A MeV Neon-20 as a Function of Depth in Water. III. Analytic Multigeneration Transport Theory. *Radiat. Res.,* **134**(1): 1-14; 1993.

Shinn, J.L., Cucinotta, F.A., Simonsen, L.C., Wilson, J.W., Badavi, F.F., Badhwar, G.D., Miller, J., Zeitlin, C., Heilbronn, L., Tripathi, R.K., Clowdsley, M.S., Heinbockel, J.H., Xapsos, M.A. "Validation of a Comprehensive Space Radiation Transport Code", *IEEE Transactions on Nuclear Science*, **45**: 2711-2719; 1998.

Tripathi, R.K., Townsend, L.W., Kahn, F. Role of intrinsic width in fragment momentum distributions in heavy ion collisions, *Phys. Rev. C.*, **48**(4), R1775-R1777; 1994.

Tweed, J., Walker, S.A., Wilson, J.W., Cucinotta, F.A., Tripathi, R.K., Blattnig, S., Mertens, C.J. Computational Methods for the HZETRN Code. *Adv. Space Res*. **35**:194-201; 2005.

Tweed, J., Walker, S.A., Wilson, J.W., Tripathi, R.K., Cucinotta, F.A., Badavi, F.F., An improved Green's function code for HZE transport. ICES SAE 2006-01-2147, 2006.

Walker, S.A., Tweed, J., Wilson, J.W., Cucinotta, F.A., Tripathi, R.K., Blattnig, S., Zeitlin, C., Heilbronn, L., Miller, J. Validation of the HZETRN Code for Laboratory Exposures with 1 A GeV Iron Ions in Several Targets. *Adv. Space Res*. **35**: 202-207; 2005.

Wilson, J.W., Khandelwal, G.S. Proton dose approximation in convex geometry. *Nucl. Tech*. **23**: 298-305;1974.

Wilson, J.W. *Analysis of the theory of high-energy ion transport*. NASA TN D-8381, 1977.

Wilson, J.W., Townsend, L.W., Bidasaria, H.B., Schimmerling, W., Wong, M. Howard, J. 20-Ne depth-dose relations in water. *Health Phys*. **46:** 1101-1111; 1984.

Wilson, J. W., Badavi, F. F., Methods of Galactic Heavy Ion Transport. *Radia. Res*. 108: 231; 1986.

Wilson, J. W.; Townsend, L. W.; and Badavi, F. F.: A Semiempirical Nuclear Fragmentation Model. *Nucl. Inst. & Methods* B**18**: 225; 1987a.

Wilson, J. W.; Townsend, L. W.; and Badavi, F. F.: Galactic Cosmic Ray Propagation in Earth's Atmosphere. *Radiat. Res*. **109**: 173-183; 1987b.

Wilson, J.W. S. Y. Chun, W. W. Buck, and L. W. Townsend: High Energy Nucleon Data Bases. *Health Phys*., **55:** 817-819; 1988.

Wilson, J.W., Lamkin, S.L., Farhat, H. Ganapol, B.D., Townsend, L.W., *A hierarchy of transport approximations for high energy (HZE) ions*. NASA TM-4118, 1989.

Wilson, J. W., Townsend, L. W., Schimmerling, W., Khandelwal, G. S., Khan, F., Nealy, J. E., Cucinotta, F. A., Simonsen, L. C., Shinn, J. L., Norbury, J. W. *Transport Methods and Interactions for Space Radiations*. NASA RP-1257, 1991.

Wilson, J. W., Shavers, M. R., Badavi, F. F., Miller, J., Shinn, J. L., and Costen, R. C., Nonperturbative Methods in HZE Propagazition. *Radiat. Res*. **140**: 241-244; 1994a.

Wilson, J. W., Townsend, L. W., Shinn, J. L., Badavi, F. F., Lamkin, S. L., Galactic Cosmic Ray Transport Methods: Past, Present, and Future. *Adv. Space Res*. **14**: (10) 841 - (10) 852, 1994b.

Wilson, J. W., R. K. Tripathi, F. A. Cucinotta, J. L. Shinn, F. F. Badavi, S. Y. Chun, J. W. Norbury, C. J. Zeitlin, L. H. Hielbronn, and J. Miller, NUCFRG2, *An Evaluation of the Semiempirical Nuclear Fragmentation Database*, NASA TP-3533, 1995.

Wilson, J. W., Cucinotta, F. A., Tai, H., Shinn, J. L., Chun, S. Y., Tripathi, R.K., Sihver, L., Transport of light ions in matter. Adv. Space Res. **21**(12): 1763-1771; 1998.

Wilson, J.W., Tweed, J., Tai, H., and Tripathi, R.K. A simple model for straggling evaluation. *Nucl Inst & Methods* B **194**: 389-392; 2002.

Wilson, J.W., Tripathi, R.K., Qualls, G.D., Cucinotta, F.A., Prael, R.E., Norbury, J.W., Heinbockel, J.H., and Tweed, J. Space Radiation Transport Methods Development, *Adv. Space Res*. **34:** 1319-1327; 2004.

Wilson, J.W., et al., A procedure for benchmarking laboratory exposures with 1 A GeV iron ions. *Adv. Space Res*. **35:** 185-193; 2005a.

Wilson, J.W., et al., International space station: A test bed for experimental and computational dosimetry. *Adv. Space Res*. **37**: 1656-1663; 2005b.

Wilson, J.W., Tripathi, R.K., Cucinotta, F.A., Badavi, F.F., *Standardized radiation shield design method: 2005 HZETRN*. SAE ICES 2006-01-2109, 2006.

Wilson, J.W., Nealy, J.E., Dachev, Ts.P., Tomov, B.T., Cucinotta, F.A., Badavi, F.F., De Angelis, G., Atwell, W., Leutke, N., Time serial analysis of the LEO environment within ISS 6A. *Adv. Space Res*. In Press, 2007.

Wong, M., Schimmerling, W., Phillips, H., Ludewigt, B.A., Landis, D., Walton, J., Curtis, S.B. The multiple coulomb scattering of very heavy charged particles. *Medical Phys*. **17**(2):163-171; 1989.

Zeitlin, C., Heilbronn, L., Miller, J., Rademacher, S.E., Borak, T., Carter, T.R., Frankel, K.A., Schimmerling, W., Stronach, C.E. Heavy fragment production cross sections from 1.05 GeV/mucleion 56Fe in C, Al, Cu, Pb, and CH2 targets. *Phys. Rev*. C**56**: 388-397; 1997.